CHAPTER- 3

Effect of palladium and its nanogeometry on the redox electrochemistry of tetracyanoquinodimethane modified electrode; Application in electrochemical sensing of ascorbic acid

3.1 Introduction

Ascorbic acid (AA) also known as vitamin C, is a water-soluble vitamin, widely present in many biological systems, fruits, and vegetables. Ascorbic acid is frequently used to replace poor dietary intake because it is a powerful antioxidant and free-radical scavenger in human metabolism and may help to prevent illnesses like cancer and Parkinson's disease. Furthermore, the deficit of ascorbic acid can result in scurvy disease. It is also used to treat a wide range of diseases, such as cancer, Alzheimer's disease, atherosclerosis, infertility, and some HIV infection-related clinical symptoms [1,2]. The identification of ascorbic acid in a wide range of natural and prepared meals, medications, physiological fluids, fruit juices, soft drinks, and vegetables is crucial for biological and agro-industrial sectors. Therefore, the determination of ascorbic acid levels in the human body, fruit juice, soft drinks, and prepared meals, has been accomplished by a variety of methods, including chemiluminescence [3,4], spectrometry [5,6], and chromatography [7,8]. However, these methodologies lack specificity and susceptibility to interference from other reducing agents in the sample. Since ascorbic acid is an electroactive compound, electrochemical techniques for its identification have garnered significant attention due to its great sensitivity, ease of use, for determining trace analytes, and affordability. These methods have been developed for a wide range of cations, anions, as well as organic compounds. Electrochemical methods, particularly voltammetry, have grown in prominence in recent years. These electrochemical methods have been used to identify pharmaceutical chemicals in dosage forms as well as biological samples [9]. The utilization of nanomaterial-modified bare electrodes as the redox-active center has been used in the fabrication and advancement of electrochemical sensing devices. Thus, the

synthesis of novel metal nanomaterials is imperative and has become a challenging research topic.

In recent decades, noble metal nanoparticles (NMNPs), including Au, Ag, Pt, Pd, Ru, and their alloys, have garnered growing interest due to their distinct electrical, magnetic, optical, and catalytic characteristics [10]. Particularly noteworthy are Pd-based catalysts, which have gained prominence due to their comparatively lower cost and enhanced sensing capability compared to Pt catalysts [11,12]. Palladium nanoparticles have been used in the development of numerous electrochemical sensors. For example, palladium nanoparticles loaded with carbon nanofiber-modified electrodes were used for the simultaneous electrochemical measurement of dopamine, uric acid, and ascorbic acid [13]. An ultrathin palladium nanowire-modified electrode for selective determination of ascorbic acid [14], and palladium incorporated poly(3,4-ethylenedioxythiophene) films for simultaneous detection of dopamine and uric acid [15]. Palladium (Pd) nanoparticles and nanostructures play a crucial role in electrochemical sensing due to their unique physicochemical properties, such as excellent catalytic activity, high surface area, and superior electron transfer capabilities. The high surface area of Pd nanoparticles provides more active sites for electrochemical reactions. Pd nanoparticles accelerate the electron transfer between the electrode and the ascorbic acid, leading to faster reaction kinetics and improved signal responses. These properties significantly enhance the detection limit and sensitivity of ascorbic acid. The aim of my research is the fabrication of palladium-modified electrodes and increase the sensitivity and low limit of detection during electrochemical sensing of ascorbic acid. Palladium nanoparticle has a high surface area so it shows high electrocatalytic activity. Due to its high catalytic activity, ascorbic acid

interacts more on the electrode surface and provides more electron and charge transfer therefore the Rct value decreases during electrochemical sensing of ascorbic acid as clearly shown in the EIS image. Pd has a stronger hydrogen affinity and superior performance than Pt in certain oxidation reactions, including alcohol and formic acid oxidation [16]. Palladium is generally more abundant and cheaper than platinum, making it a more economical choice for applications. Pd has more electrocatalytic activity and electrocatalytic stability than Pt [17]. Pd is more resistant to carbon monoxide (CO) poisoning than Pt, which is a significant advantage in catalysis and sensing. Pt sensors often suffer from CO poisoning, which hinders their performance in real-time applications. [18,19] Silver is cheaper than Pd, but its lower catalytic activity and tendency to oxidize in air and aqueous environments reduce its practicality in many catalytic and sensing applications. In conclusion, Pd nanoparticles offer a balance of high catalytic activity, cost-effectiveness, and good stability, especially in applications that involve hydrogen. Their resistance to poisoning and ability to form stable composites make them highly advantageous in electrochemical sensing compared to Pt and Ag. The electron transfer rate of nanoparticles in electrochemical sensing is primarily influenced by the size, shape, and electronic properties of the material. Palladium nanoparticles are widely used due to their excellent catalytic activity, surface area, and conductivity, which enhance the electron transfer process. However, comparing the electron transfer rates of Pd NPs with other nanoparticles such as gold (Au), platinum (Pt), and transition metal oxides (NiO) provides insights into their efficiency in different electrochemical applications. Palladium-modified electrodes exhibit lower charge transfer resistance and improved catalytic efficiency, making them ideal for application in the sensing of

biomolecules [20]. Au NPs have lower electron transfer kinetics for hydrogen evolution reaction compared to Pd NPs but are still competitive in glucose oxidase-based biosensors [21]. Pt NPs show comparable electron transfer kinetics in HER and ORR compared to Pd NPs, but their higher cost and susceptibility to poisoning (e.g., by CO) are significant drawbacks [22]. NiO-modified electrodes show slower electron transfer compared to Pd NPs, but are still effective for non-enzymatic glucose sensing due to the strong electrocatalytic activity in alkaline solutions [23]. The incorporation of graphene oxide enhances the electron transfer kinetics of Pd NPs, making them superior to conventional nanoparticles [24].

Tetracyanoquinodimethane (TCNQ) with four cyano groups and π conjugation bonds have facilitated the formation of organic charge-transfer complexes and ion-radical salts like K (TCNQ) and Na (TCNQ) [25–31]. TCNQ has also been used as a redox mediator for regenerating oxidoreductase enzymes, especially glucose oxidase, and peroxidase, including the cofactor participating with dehydrogenase enzyme [32–35]. The advantage of the organic redox mediator is low background current even at a higher quantity within graphite paste which in turn allows sensitive and precise probing of various enzymatic reactions [36]. This justified the potential utilization of TCNQ in electrochemical biosensing. Although TCNQ has numerous advantages with electrochemical sensing, the dynamics of electrochemical reaction between biocatalyst and TCNQ is relatively slower as compared to that recorded with ferrocene derivative under similar conditions. This necessitated the search for a novel way to enhance the electrochemical performances of TCNQ as a redox mediator for a variety of practical applications on electrocatalysis, as attempted in the current study.

The redox electrochemistry of the electron transfer mediator within a heterogeneous matrix has been shown to be dependent on the support morphology. The redox electrochemistry becomes sluggish on the exploitation of a nanostructured matrix for redox molecule encapsulation [37]. The sluggish electrochemistry related to the redox mediator encapsulated nanostructured matrix is due to the restricted mobility of the redox couple within the heterogeneous phase. This directed the current study toward a possible approach to fastening the rate of bio-electrochemical interaction between enzyme and redox mediators for reliable and sensitive electrochemical sensing. Herein, an attempt was made to introduce palladium into organically modified silicate (ORMOSIL) precursors as a heterogeneous matrix, involving the active role of palladium chloride [38]. This involved a specific interaction between palladium chloride and precursors of ORMOSIL, i.e., 3-glycidoxypropyltrimethoxysilane (GPTMS) and trimethoxysilane (TMS). GPTMS allowed the reduction of palladium chloride into palladium nanoparticles, followed by triggering the formation of palladium-linked ORMOSIL. While TMS enabled the formation of the Pd-Si-bond within the ORMOSIL matrix. These interactions between precursors of organically modified silica in the presence of ferrocene monocarboxylic acid enabled the formation of palladium-embedded ORMOSIL resulting in excellent redox electrochemistry of ORMOSIL encapsulated ferrocene derivative, and a nanostructured-heterogeneous-matrix behaving as a solid solution during electrochemical biosensing [37,39]. However, it is required to find either analogous variation in the redox electrochemistry of TCNQ that could be recorded as a function of palladium and its nanogeometry, as studied in the current work.

In current work, the use of functional alkoxysilane, especially 3-aminopropyltrimethoxysilane (3-APTMS) which allowed controlled conversion of palladium-positive ions into palladium nanoparticles with cyclohexanone [40] and formaldehyde [41], is demonstrated. The resultant palladium nanoparticles can be calcined at the desired temperature and can be incorporated within graphite paste with TCNQ to reveal the dependence of palladium on the redox electrochemistry of TCNQ. Furthermore, the nanogeometry of palladium nanoparticles can also be controlled simply by altering the amount of 3-APTMS. Therefore, palladium nanoparticles with two different nanogeometry are prepared and employed for incorporation in graphite paste along with TCNQ for finding the dependence of palladium and its nanogeometry on redox electrochemistry of TCNQ modified electrode. The study involved cyclic voltammetry, impedance spectroscopy, and a typical case of ascorbic acid electrochemical sensing for confirming the effect of palladium and its nanogeometry on redox electrochemistry of TCNQ modified electrode.

3.2 Experimental

3.2.1 Materials

Tetracyanoquinodimethane TCI India Pvt. Ltd. while graphite powder (particle size < 20 μm), Nujol oil (density 0.838 g/mL), potassium tetrachloropalladate (II) [K_2PdCl_4] were purchased from Sigma Aldrich Chemical Co., India. Formaldehyde and ascorbic acid were purchased from Merck, India. The other reagents used were all of the analytical grades and were used without further purification.

3.2.2 Synthesis of palladium nanoparticles (PdNPs)

The synthesis of PdNPs was done by a previously reported method with slight modification [40]. Briefly, 100 µL ethylene glycol solution of K_2PdCl_4 (20 mM) was mixed with 5 µL and 10 µL of 3- APTMS (10 mM) for PdNP-1 and PdNP-2, respectively. The resultant solution was mixed on a cyclo mixture followed by the addition of formaldehyde and further stirring for 10 minutes. The resultant product was incubated in a microwave for about one minute and centrifuged at 6000 rpm for 10 minutes to obtain the black color residue. The residue was washed two to three times and vacuum oven-dried at 80 ℃ for two hours.

3.2.3 Fabrication of modified carbon paste electrode

The synthesized PdNP-1 and PdNP-2 were adsorbed on graphite powder. In order to prepare the graphite-blended PdNPs, 100 µL of PdNPs solution was mixed with 100 mg of graphite powder (molecular measure < 20 µM), and the mixture was then ultrasonically processed at 20 kHz for 20 minutes. The blends were allowed to stand overnight at 80 ℃ to dry completely. To eliminate the organic components, the PdNPs adsorbed on graphite particles were calcined at 600 ℃ in an N_2 atmosphere. The calcined PdNP-1/PdNP-2 mixed with TCNQ and graphite powder in a mortar after that added a few drops of nujol oil and homogeneously mixed. The homogeneous mixture was smoothed on butter paper and a modified carbon paste was obtained. Now this modified carbon paste is filled in a melting point glass capillary, and a copper wire is connected. Now our modified carbon paste electrode is ready and used for electrochemical analysis. The composition of the modified electrode is illustrated in Table 3.1.

Table 3.1 Composition of modified carbon paste electrodes.

System	TCNQ (w/w) %	PdNPs adsorbed on graphite (w/w) %	Graphite (w/w) %	Nujol oil (w/w) %
TCNQ	4.2	-	70.8	25.0
CPE/TCNQ-PdNP-1	4.2	10.0	60.8	25.0
CPE/TCNQ-PdNP-2	4.2	10.0	60.8	25.0

To scaling up the electrode fabrication process for commercial or industrial applications is feasible for the following reasons:

- The material used in the fabrication of the electrode is cost-effective and easily available. Palladium is more expensive in comparison to the other metals, but the amount of PdNPs used in the modification is minimal due to their nanoscale size which makes it cost-effective.
- The synthesis method of PdNPs is simple and less time is required.
- This fabrication process is repeatable and controlled, making it ideal for mass production. For larger-scale production, automated techniques such as spray coating or inkjet printing can be adapted to uniformly apply TCNQ-PdNPs onto screen-printed electrode surfaces. This will increase productivity while maintaining consistency.
- For commercial applications, the process can be adapted for the fabrication of microelectrodes or screen-printed electrodes (SPEs), making it ideal for portable or disposable sensor technologies. This adaptability to miniaturization is essential for developing point-of-care diagnostics and field-based sensors.

Overall, the fabrication method of CPE/TCNQ-PdNPs is well-suited for the production of low-cost electrochemical sensors for the detection of ascorbic acid and various other electrochemical applications.

3.2.4 Electrochemical measurements

For electrochemical studies, an electrochemical workstation model, CHI 660E Inc., TX, USA, was utilized with a three-electrode cell with a working volume of 2 mL. As the reference and auxiliary electrodes, a silver/silver chloride electrode (Orion, Beverly, MA, USA) and a Pt electrode were used. The Ag/AgCl electrode is connected to all the potentials indicated below. The working electrode is a modified CPE/TCNQ, CPE/TCNQ-PdNP-1, and CPE/TCNQ-PdNP-2 electrode. The influence of sweep rates on peak current (I) was investigated by recording cyclic voltammograms at various sweep rates ranging from 1 mV/s to 500 mV/s the absence and presence of ascorbic acid, and amperometry in a 0.1 M phosphate buffer (pH 7.0).

3.3 Results and Discussion

3.3.1 Synthesis and Characterization of palladium nanoparticles

The current study revealed the preparation of nanosized palladium particles i.e., PdNP-1 and PdNP-2 of varying size with different concentrations of 3-APTMS. The XRD spectrum as shown in Figure 3.1 confirmed the planes of palladium assigned to 2θ values as per JCPDS #87-0641, corresponding to 40.02° (111), 46.49° (200), 68.05° (220), 81.74° (311), and 86.24° (222). The sharp peaks were observed for larger-size palladium nanoparticles, while the broader peaks were for smaller-size PdNPs.

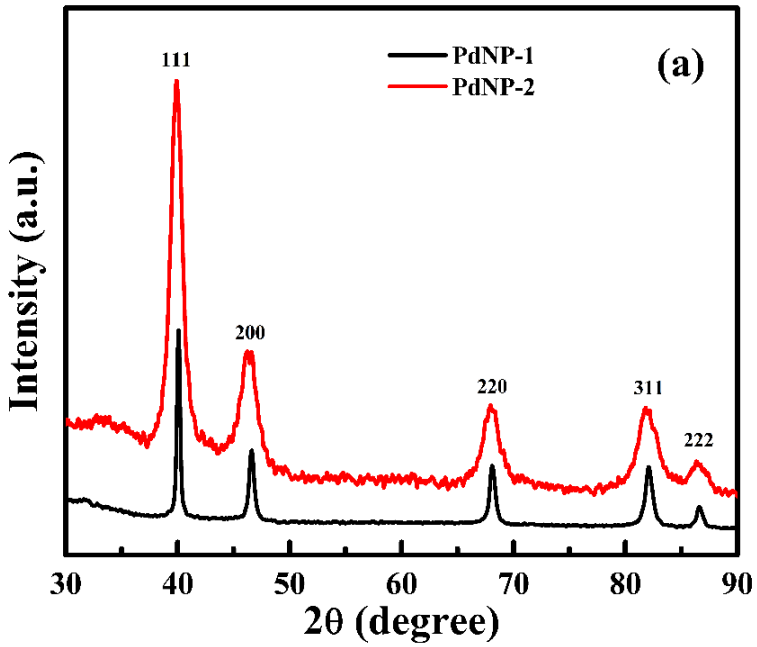

Figure 3.1 XRD spectra of palladium nanoparticles.

The surface morphology and particle sizes of PdNP-1 and PdNP-2 were analyzed using transmission electron microscopy. The TEM image of PdNP-1 depicts a nearly spherical morphology with agglomerated particles and the average particle size is in the range of 18 to 20 nm as shown in Figure 3.2 (a) and (b), respectively. The TEM image of PdNP-2 displays spherical and triangular shapes (Figure 3.2 c), with an average particle size of 8-10 nm (Figure 3.2 (d)).

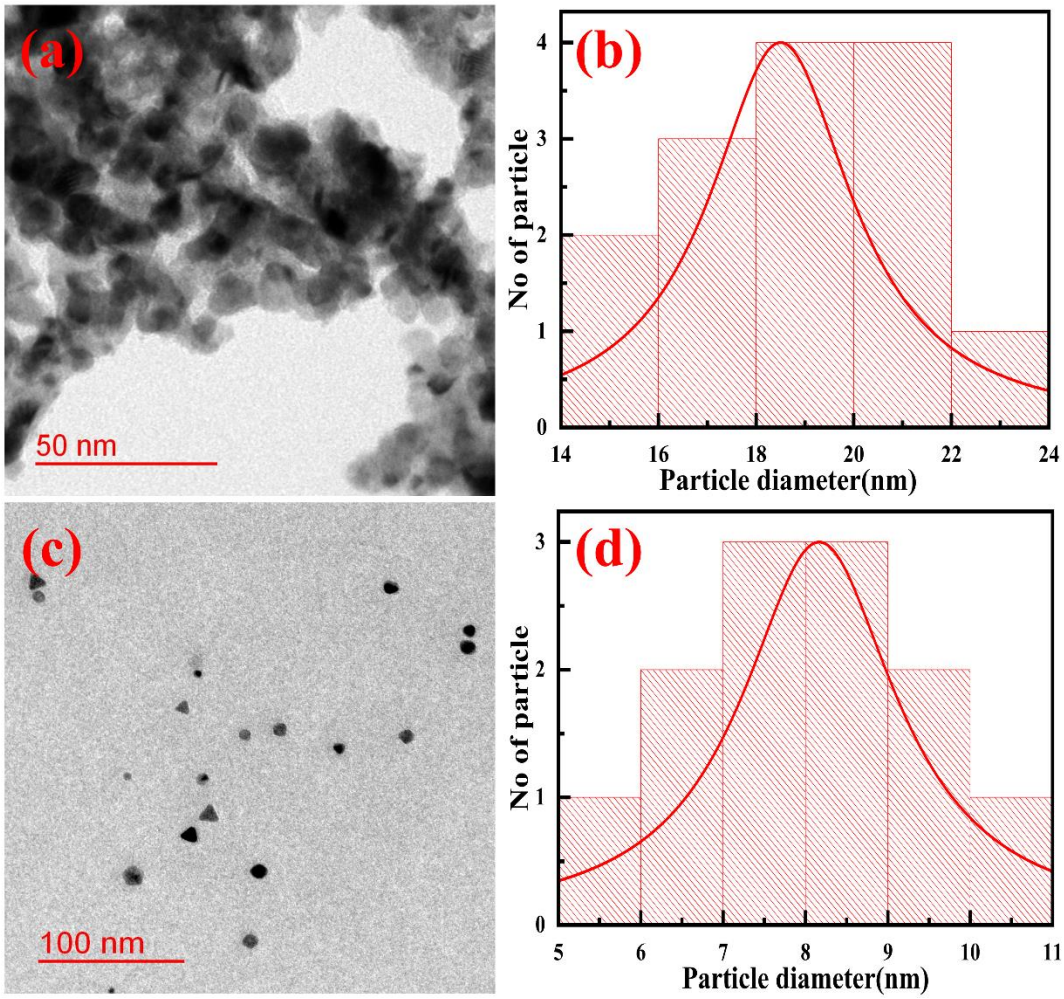

Figure 3.2 (a, c) TEM image and (b, d) particle size distribution histogram of PdNP-1 and PdNP-2, respectively.

The AFM images of PdNP-1 and PdNP-2 are illustrated in Figure 3.3 (a, b & c) and 3.3 (d, e & f), respectively. The average grain size of PdNP-1 and PdNP-2 is found to be 1 µm and 0.2 µm, respectively. These nanoparticles are used to mix with TCNQ for making modified electrodes, namely CPE/TCNQ-PdNP-1 and CPE/TCNQ-PdNP-2 for studying the impact of PdNPs on the redox electrochemistry of TCNQ.

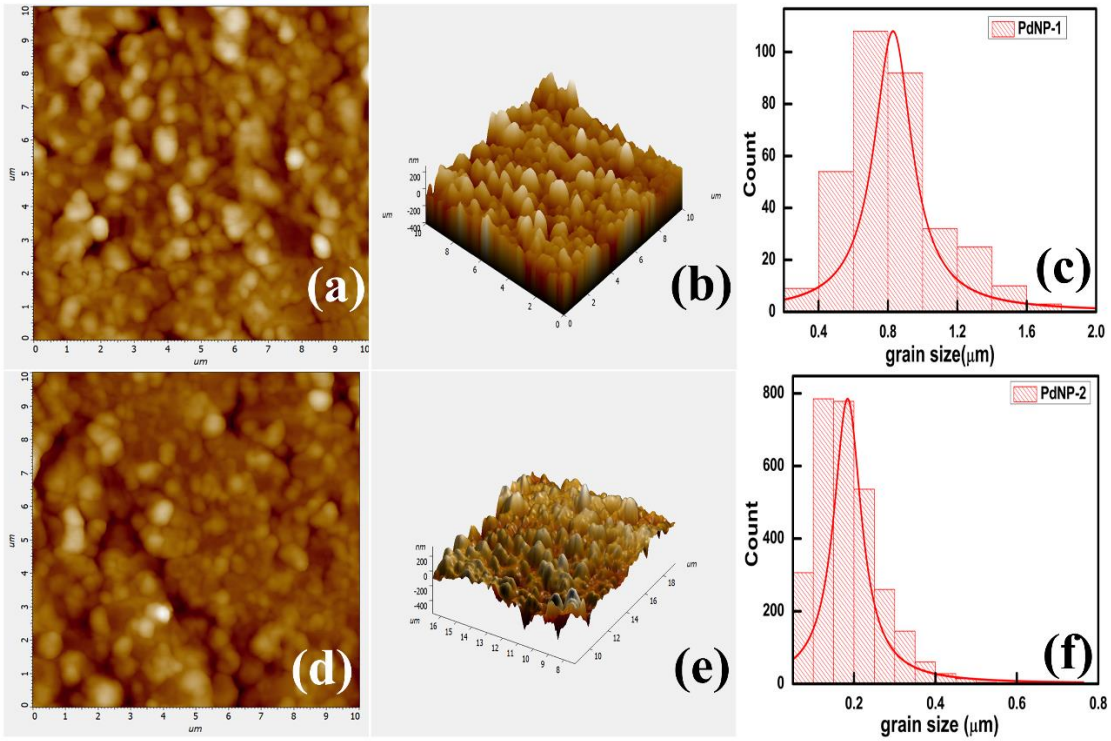

Figure 3.3 (a, d) 2D AFM image, (b, e) 3D image, and (c, f) histogram of PdNP-1 & PdNP-2, respectively.

3.3.2 Impact of Pd-nanogeometry on the redox electrochemistry of TCNQ-modified carbon paste electrodes

After carefully adsorbing PdNP-1 and PdNP-2 on graphite powder, 3-APTMS stabilized nanoparticles were calcined at 600 °C to remove all organic parts present on the palladium nanoparticle. Calcinated nanoparticles were subsequently used to understand the impact of PdNPs on the electrochemistry of TCNQ-modified electrodes as a close contact of PdNPs and TCNQ within graphite paste may facilitate the charge transfer rate during electrochemical measurements. In this regard, interesting findings were recorded. Figure 3.4 illustrates the results of cyclic voltammetry of (a) CPE/TCNQ, (b) CPE/TCNQ-PdNP-1, and (c) CPE/TCNQ-PdNP-2 with the modified carbon paste electrode (CPE). Firstly, the

variation in the redox performance of TCNQ within the CPE as a response to incorporated calcined PdNP-1 and PdNP-2 was investigated at different scan rates. As we increase the scan rate peak current increases and the oxidation peak potential is shifted towards a more positive value and the reduction peak potential shifted towards less potential. The difference in anodic (E_{pa}) and cathodic (E_{pc}) peak potentials (ΔE_p) decrease and are found to be 243 mV, 233 mV, and 231 mV for CPE/TCNQ, CPE/TCNQ-PdNP-1, and CPE/TCNQ-PdNP-2, respectively. These findings indicate the increase in electron transfer is due to the function of palladium nanogeometry.

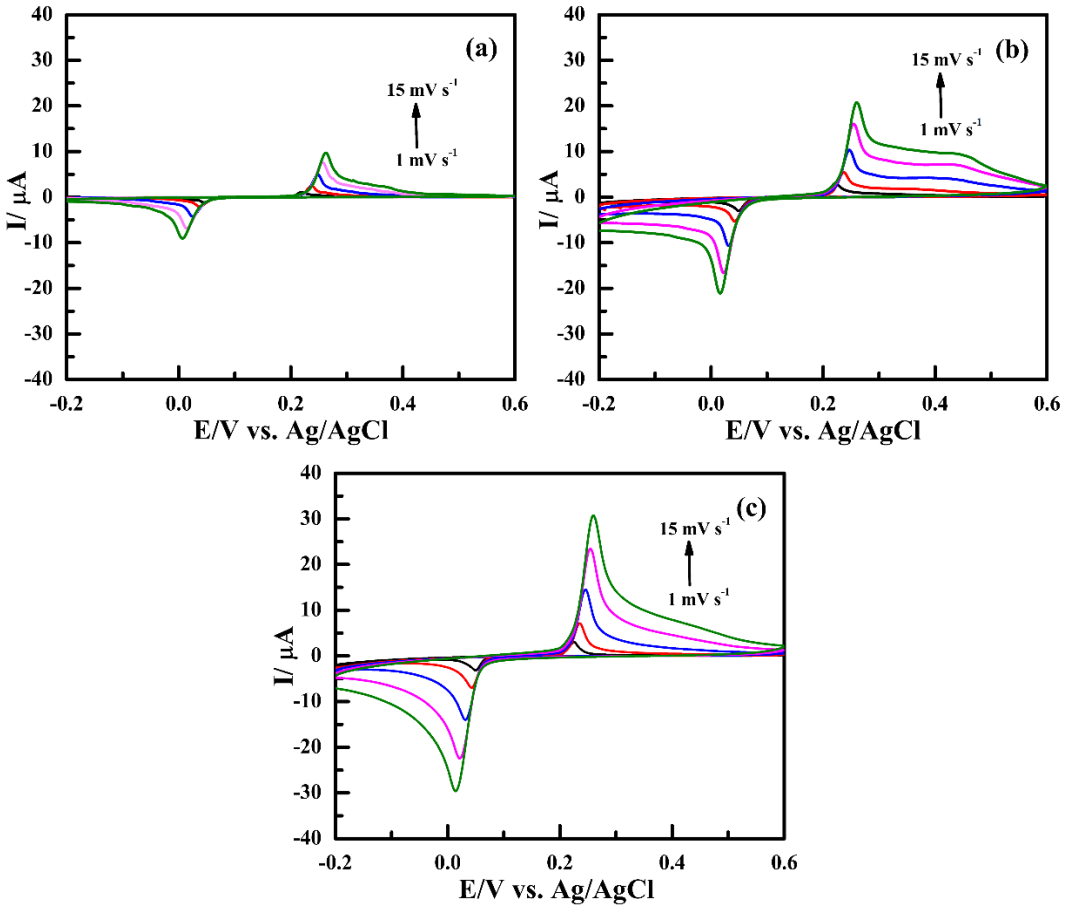

Figure 3.4 Cyclic voltammograms of (a) CPE/TCNQ (b) CPE/TCNQ-PdNP-1 and (c) CPE/TCNQ-PdNP-2 in 0.1 M PBS (pH 7.0) between -0.2 to 0.6 V vs Ag/AgCl at different scan rates.

The effect of different scan rates has been examined on the modified electrode to access the interfacial kinetics by varying the scan rate from 1 mV s^{-1} to 100 mV s^{-1} as illustrated in Figure 3.5 (a), (b), and (c) for CPE/TCNQ, CPE/TCNQ PdNP-1, and CPE/TCNQ PdNP-2 respectively. The plot of the oxidation peak current and reduction peak current versus the square root of the scan rate ($\upsilon^{1/2}$) gave a linear relationship, indicating that the reaction at the electrode-electrolyte interface is the diffusion control process.

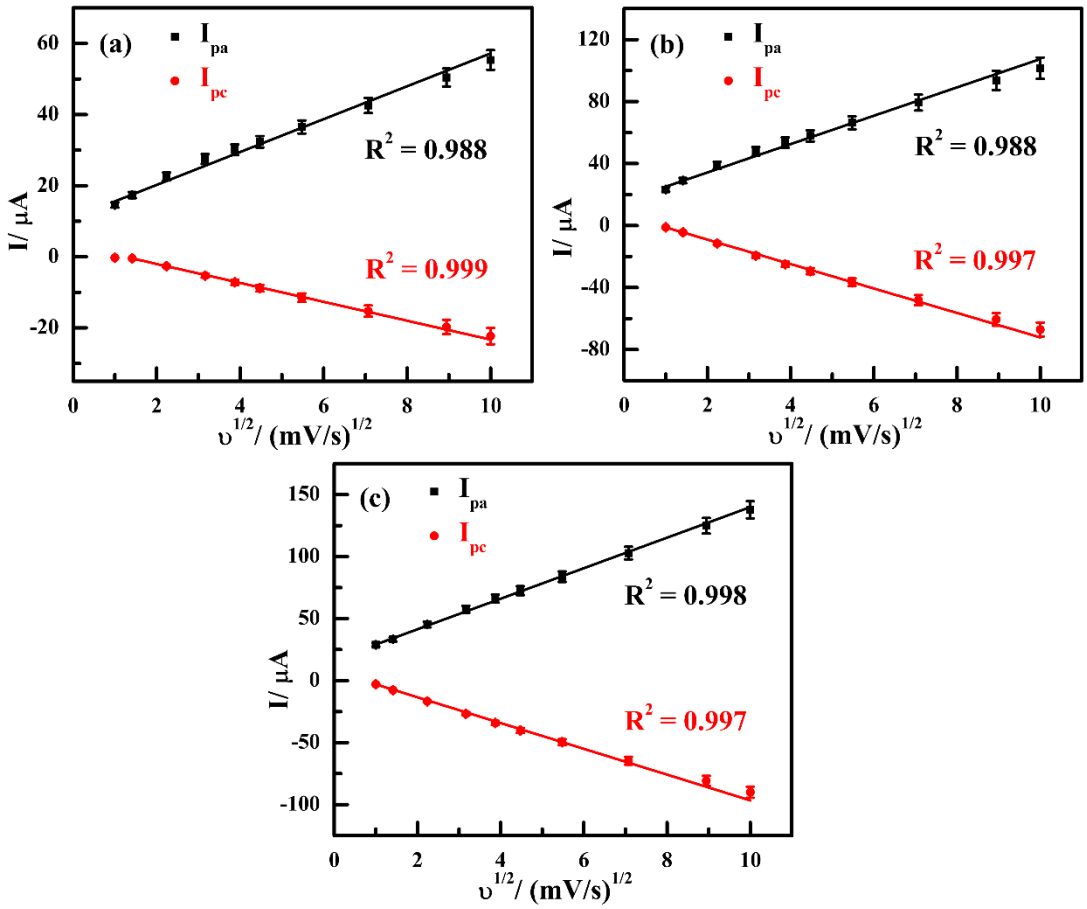

Figure 3.5 A plot of anodic/cathodic current versus square root of the scan rate for (a) CPE/TCNQ (b) CPE/TCNQ-PdNP-1 and (c) CPE/TCNQ-PdNP-2.

Subsequently, the dynamic electrochemistry was investigated based on cyclic voltammetry in the absence and the presence of varying concentrations of ascorbic acid which act as an efficient electroactive species for direct and mediated electrochemistry.

The results, as shown in Figure 3.6, clearly revealed the significant enhancement of anodic current attributed to the electrochemical transformation of ascorbic acid which in turn confirmed the increase in electron transfer i.e. reduction in charge transfer resistance as a function of palladium nanogeometry.

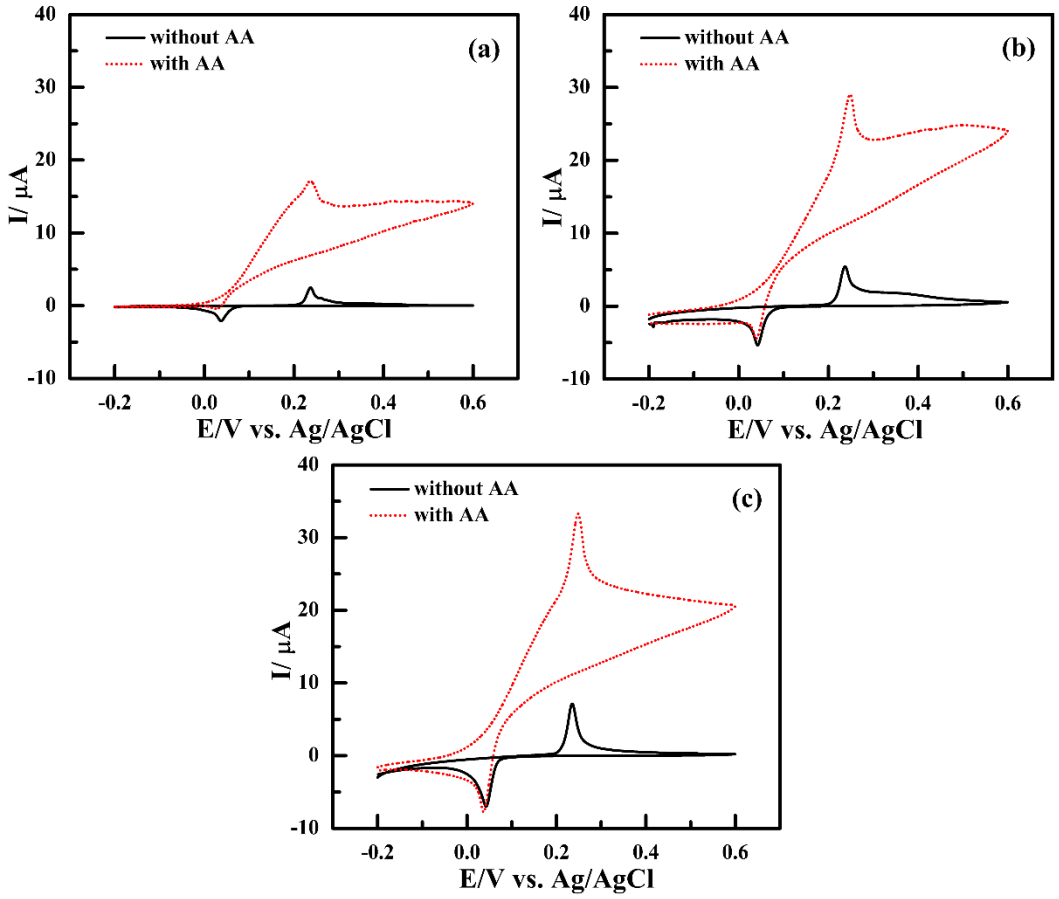

Figure 3.6 Cyclic voltammograms of (a) CPE/TCNQ (b) CPE/TCNQ-PdNP-1 and (c) CPE/TCNQ-PdNP-2 in the absence and presence of ascorbic acid (625 µM) in 0.1 M PBS (pH 7.0) at a 2 mV/s scan rate.

Further to understand the impact of palladium and its nanogeometry we plotted a graph current function ($I_{pa}/\upsilon^{1/2}$) versus the square root of scan rate ($\upsilon^{1/2}$) as shown in Figure 3.7 (a), (b), and (c). It has been found that all three electrodes such as CPE/TCNQ, CPE/TCNQ-PdNP-1, and CPE/TCNQ-PdNP-2 in the absence of ascorbic acid show a

horizontal straight line, whereas on the addition of ascorbic the current function gradually decreases as an increase in scan rate and finally tend to a straight line. At a higher scan rate, it attained equilibrium, and a steady-state current was obtained. The current function attains a steady value at a relatively higher scan rate in CPE/TCNQ-PdNP-2 as compared to CPE/TCNQ-PdNP-1 and CPE/TCNQ justifying faster charge transfer dynamics as a function of palladium nanogeometry.

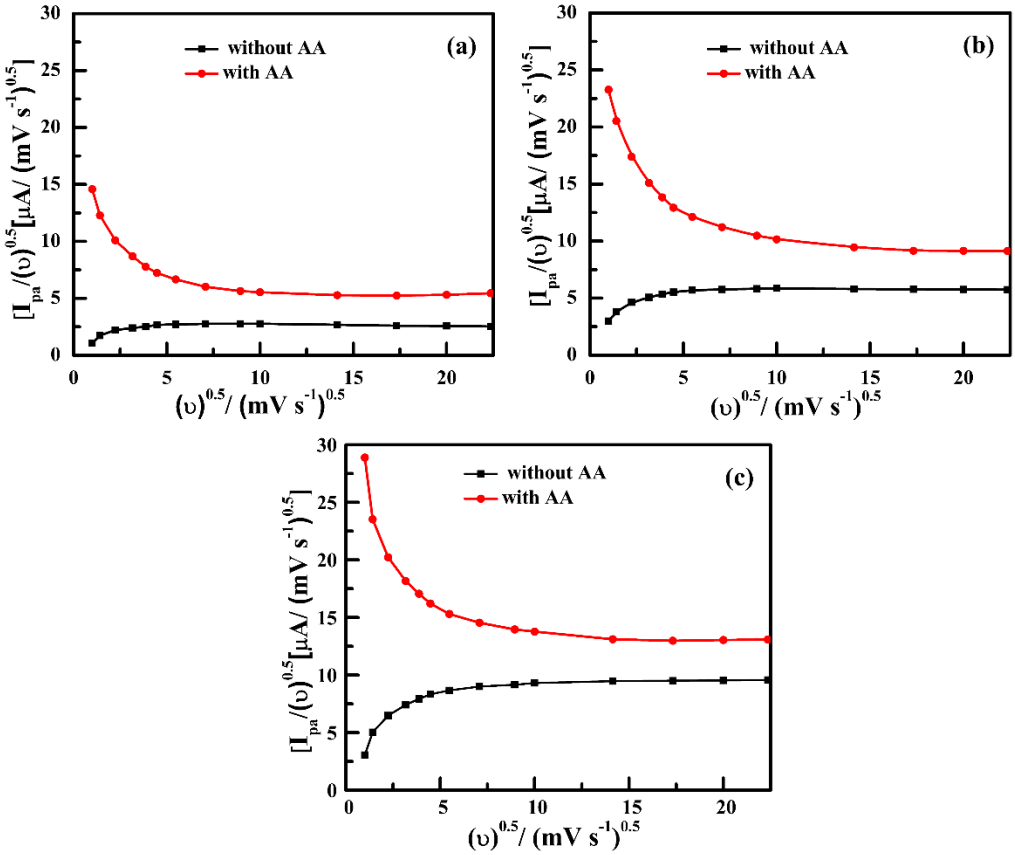

Figure 3.7 The plot of current function vs square root of scan rate of (a) CPE/TCNQ (b) CPE/TCNQ-PdNP-1 and (c) CPE/TCNQ-PdNP-2.

Differential pulse voltammetry (DPV) was subsequently investigated to understand the impact of palladium and its nanogeometry during electrochemical sensing. Figure 3.8 (a), b), and (c) shows the differential pulse voltammograms at varying concentrations of

ascorbic acid ranging from 0 mM to 5 mM for CPE/TCNQ, CPE/TCNQ-PdNP-1, and CPE/TCNQ-PdNP-2, respectively. The peak potential for ascorbic acid oxidation was found at around 0.247 V, 0.250 V, and 0.262 V for CPE/TCNQ, CPE/TCNQ-PdNP-1, and CPE/TCNQ-PdNP-2, respectively. The magnitude of peak current also increases with increasing the concentration of ascorbic acid.

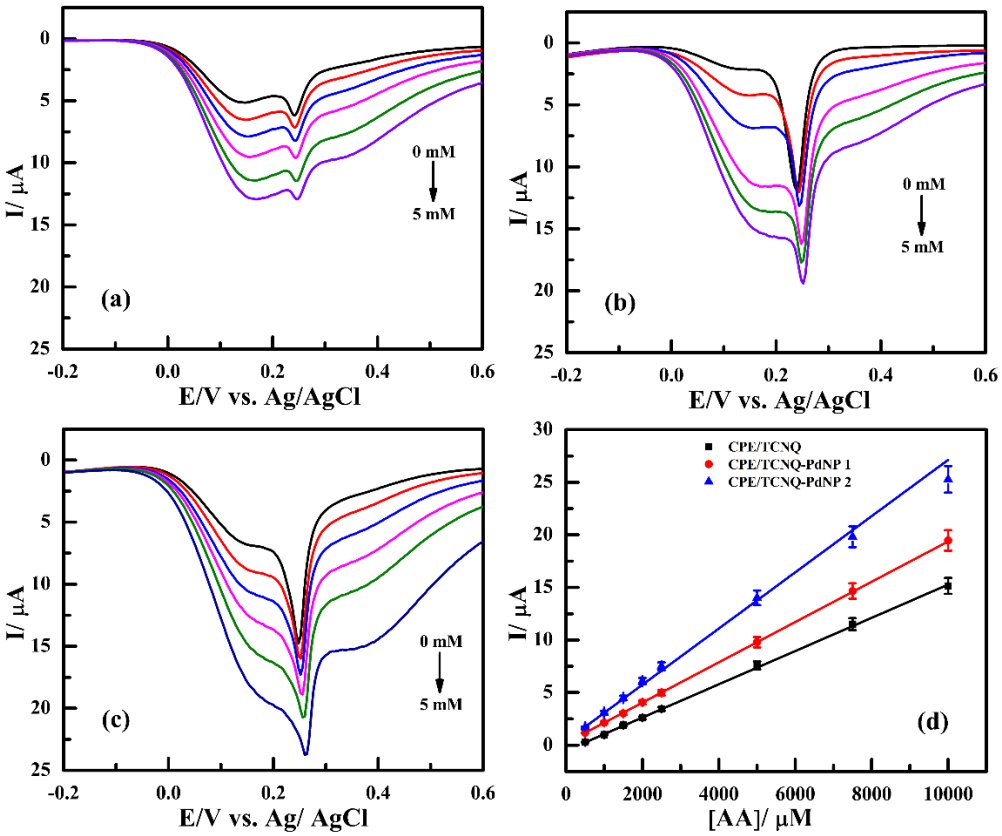

Figure 3.8 Differential pulse voltammograms of (a) CPE/TCNQ (b) CPE/TCNQ-PdNP-1 (c) CPE/TCNQ-PdNP-2 in the presence of varying concentrations of ascorbic acid. (d) shows the linear relation between peak current vs concentration of ascorbic acid.

Figure 3.8 (d) shows the calibration curve of current versus ascorbic concentration. A linear relationship was obtained between the differential pulse voltammetry current and AA concentration with a gradual increase in sensitivity of AA sensing and found to be 1.5, 1.9, and 2.5 µA/mM for CPE/TCNQ, CPE/TCNQ-PdNP-1, and CPE/TCNQ-PdNP-

2 electrodes, respectively again confirming the contribution of palladium and its nanogeometry.

The finding recorded in Figure 3.9 was further examined for reliable electrochemical sensing of ascorbic acid based on static electrochemistry at a constant potential close to the redox potential of CPE/TCNQ, CPE/TCNQ-PdNP-1, and CPE/TCNQ-PdNP-2 electrodes. Electroanalytical performances of modified electrodes were performed by amperometric measurement under stirring conditions. Amperometric measurement was performed successively by adding ascorbic acid (50 µM to 625 µM) to the continuously stirred solution with a working potential of 0.22 V versus Ag/AgCl and recorded. CPE/TCNQ-PdNP-2 showed higher current responses than CPE/TCNQ-PdNP-1 and CPE/TCNQ modified electrodes, as shown in Figure 3.9 (a), (b), and (c). The standard curve prepared for ascorbic acid (AA) detection by amperometry is shown in Figure 3.9 (d). The outcomes imply an extensive linear relationship between the amperometric current and AA concentration. The limit of detection (LOD) was calculated by using the equation (3.1).

$$\mathbf{LOD = 3 * SD/m} \tag{3.1}$$

Where SD is the standard deviation in the intercept and m is the slope of the calibration curve. The LOD was determined to be 51.61 µM, 44.38 µM, and 30.10 µM for CPE/TCNQ, CPE/TCNQ-PdNP-1, and CPE/TCNQ-PdNP-2 modified electrodes, respectively [42]. The sensitivity for AA sensing was found to be 5, 7.5, and 14.8 µA/mM for CPE/TCNQ, CPE/TCNQ-PdNP-1, and CPE/TCNQ-PdNP-2 electrodes, respectively.

This confirms that the nanogeometery of palladium plays a significant role in the electroanalysis of AA.

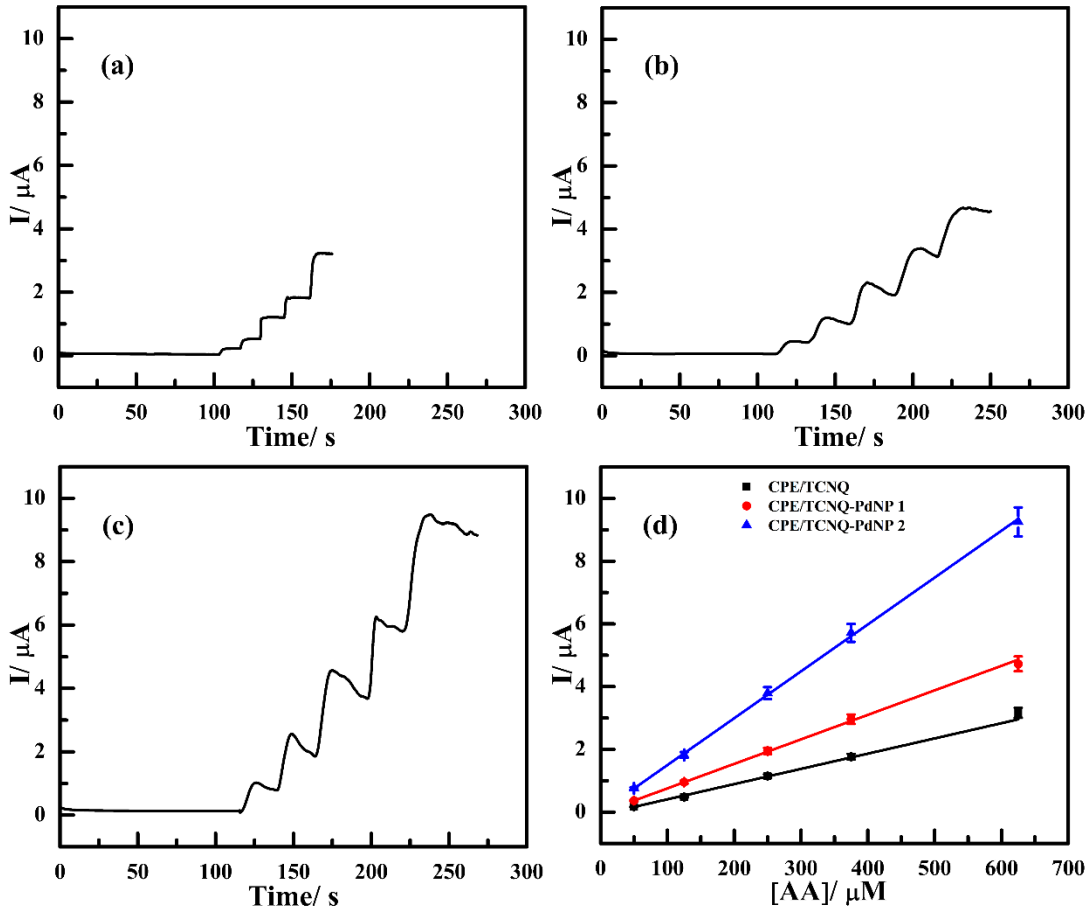

Figure 3.9 Amperometric response of (a) CPE/TCNQ (b) CPE/TCNQ PdNP-1 and (c) CPE/TCNQ PdNP-2 on the addition of varying concentrations of ascorbic acid between (50 µM to 625 µM) recorded at a constant potential of 0.22 V vs Ag/AgCl. (d) shows the linear relation between peak current vs concentration of ascorbic acid.

3.3.3 Electrochemical impedance spectroscopy

EIS study was further performed to examine the impact of palladium and its nanogeometry on electrode-electrolyte interface in the 0.1 M PBS (7.0 pH). The EIS analysis was recorded for CPE/TCNQ, CPE/TCNQ-PdNP-1, and CPE/TCNQ-

PdNP-2 electrodes in 0.1 M phosphate buffer between the frequency range of 1.0 Hz to 1000 kHz as shown in (Figure 3.10).

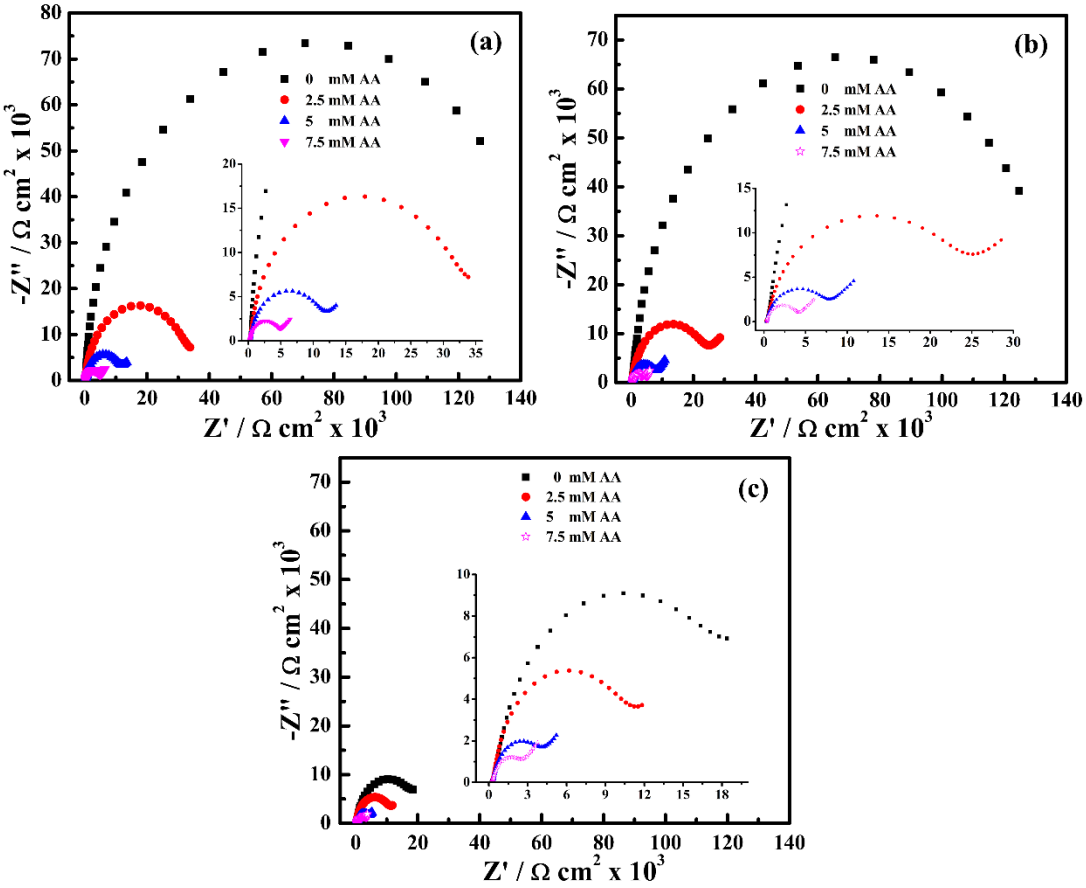

Figure 3.10 Nyquist plots of (a) CPE/TCNQ (b) CPE/TCNQ-PdNP-1 and (c) CPE/TCNQ-PdNP-2 in the presence of (0 mM to 7.5 mM) ascorbic acid.

The EIS data was fitted on R(CR)W circuit by using ZSimpWin software. A typical Nyquist plot for Randle's circuit has two parts: the semi-circular and the linear element. At low frequencies, the linear element represents the mass transfer diffusion, whereas, at high frequencies, the semicircle's diameter signifies the charge transfer resistance (R_{ct}) [43]. The diameter of the circle component inside the Nyquist plot represents the charge transfer resistance (R_{ct}) of the system. CPE/TCNQ-PdNP-2 shows

reduced R_{ct} (2.73 x 10^3) Ω cm^2 in comparision to the CPE/TCNQ-PdNP-1 (4.55 x 10^3) Ω cm^2 and CPE/TCNQ (5.66 x 10^3) Ω cm^2, respectively, in the presence of 11.25 mM AA concentration which indicates that the maximum charge transfer takes place in CPE/TCNQ-PdNP-2. This may be due to the increase in the surface area of the electrode and variable shapes of the as-synthesized PdNP-2.

Table 3.2 Comparison of charge transfer resistance.

	CPE/TCNQ	**CPE/TCNQ-PdNP-1**	**CPE/TCNQ-PdNP-2**
Concentration of AA (mM)	R_{ct} (Ω cm^2)	R_{ct} (Ω cm^2)	R_{ct} (Ω cm^2)
0 (blank)	150.00 x 10^3	135.00 x 10^3	22.15 x 10^3
3.75	32.00 x 10^3	25.18 x 10^3	11.37 x 10^3
7.50	11.66 x 10^3	8.85 x 10^3	4.03 x 10^3
11.25	5.66 x 10^3	4.55 x 10^3	2.73 x 10^3

Additionally, with an increase in the concentration of ascorbic acid, the diameter of the semicircle decreases, and so does the gradual increase in the charge transfer process. The values of charge transfer resistance for CPE/TCNQ, CPE/TCNQ-PdNP-1, and CPE/TCNQ-PdNP-2 electrodes were calculated as recorded in Table 3.2, clearly justifying the impact of palladium and its nanogeometry on the redox electrochemistry of TCNQ confirming that an increase in palladium nanogeometry subsequently decreases the charge transfer resistance allowing faster dynamic electrochemistry of TCNQ modified electrode.

Table 3.3 Comparison of proposed modified carbon paste electrodes with previously reported ascorbic acid sensors.

Electrode	Linear range (µM)	LOD (µM)	Sensitivity (µA/mM)	Reference
$MnFe_2O_4/MoS_2$/SPCE	200-1000	175.0	-	[44]
ERGO/GCE	500-2000	250.0	-	[45]
GO-$TmPO_4$/GCE	100-1000	39.0	12.39	[46]
PANI/SPE	30-270	30.0	17.7	[47]
NiHCF/Au	100-12000	25.0	-	[48]
PrGO/PB/GCE	283-2330	34.7	-	[49]
ZnO-CuxO-PPy/GCE	200-1000	25.0	-	[50]
CPE/TCNQ	50-625	51.61	5.0	This work
CPE/TCNQ-PdNP-1	50-625	44.38	7.5	This work
CPE/TCNQ-PdNP-2	50-625	30.35	14.8	This work

(SPCE = screen printing carbon electrode, GCE = glassy carbon electrode, PANI = Polyaniline NiHCF = Nickel hexacyanoferrate, PPy = poly payroll, PB = Prussian blue)

3.3.4 Calculation of electrochemical active surface area

The electrochemical active surface area (EASA) of working electrodes was investigated by taking a cyclic voltammogram of CPE/TCNQ, CPE/TCNQ-PdNP-1, and CPE/TCNQ-PdNP-2 in 0.1 M phosphate buffer at a scan rate of 15 mV/s, which is shown in (Figure 3.4 (a), (b), and (c), respectively. Peak current increases with increasing scan rate and the oxidation peak potential is shifted to a more positive value and the reduction peak

potential is shifted to a lower potential. To determine the EASA of CPE/TCNQ, CPE/TCNQ-PdNP-1, and CPE/TCNQ-PdNP-2, we utilized the Randles-Sevcik equation [51] described in equation (3.2).

$$\mathbf{I_p = (2 \cdot 69 * 10^5) n^{3/2} A D^{1/2} \nu^{1/2} C_0} \quad (3.2)$$

Where A denotes the electrochemical active surface area (cm^2), D denotes the diffusion coefficient of ascorbic acid (5.0 x 10^{-6} cm^2 s^{-1} at 25 °C), C_0 denotes the concentration of electroactive analyte, n denotes the number of electrons exchanged during the reversible reaction, I_p denotes peak current (A), and υ denotes the scan rate (Vs^{-1}). By putting these values in equation (1), the EASA of CPE/TCNQ, CPE/TCNQ-PdNP-1, and CPE/TCNQ-PdNP-2 were calculated to be 0.0547 cm^2, 0.2350 cm^2, and 0.2704 cm^2 respectively. The electrochemical characterizations indicate that CPE/TCNQ-PdNP-2 has superior electrochemical behavior than CPE/TCNQ and CPE/ TCNQ-PdNP-1. It is predicted that CPE/TCNQ-PdNP-2 to be a good platform for the electrochemical sensing of ascorbic acid.

3.3.5 Effect of pH on CPE/TCNQ-PdNP-2, reproducibility and stability

The pH parameter is extremely important for the electrochemical sensing of AA since it strongly influences the oxidation process. The electrochemical response of AA was studied by using cyclic voltammetry technique in 0.1 M phosphate buffer solution with different pH values (5.0 pH to 9.0 pH). It has been observed that at pH 7.0 highest current was obtained due to the anodic oxidation of AA (Figure 3.11 (a)). Thereafter, either an increase or decrease in the pH value has decreased the peak current, and the standard deviation in the current was 1.89 %.

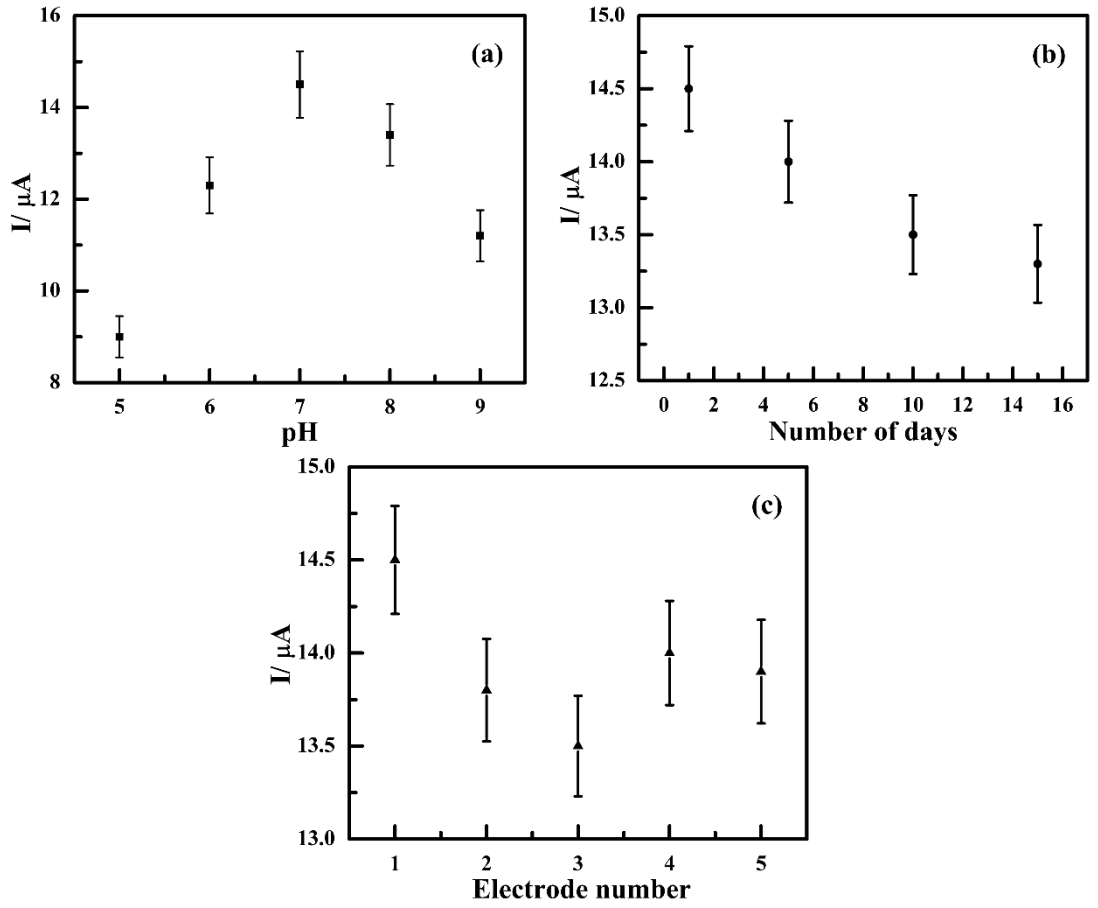

Figure 3.11 (a) Effect of pH on CPE/TCNQ-PdNP-2 modified electrode (b) stability and (c) reproducibility of CPE/TCNQ-PdNP-2 modified electrodes.

The stability of the modified electrode was checked by storing the electrode at ambient temperatures for 5, 10, and 15 days. After then cyclic voltammetric analysis was performed in 0.1 M phosphate buffer solution (pH 7.0). The decrease in the current was found to be 98 %, 96 %, and 94 % of its initial value (Figure 3.11 (b)). This result shows that modified electrodes have good stability.

To determine the sensor's reproducibility, five independent CPE/TCNQ-PdNP-2 modified electrodes were produced in the same manner, and cyclic voltammetric analysis was performed in 0.1 M phosphate buffer solution (pH 7.0). The variation in the current

was only 1 μA (Figure 3.11 (c)). The standard deviation was 0.35 % indicating that the modified electrode is showing good reproducibility.

3.3.6 Real sample analysis

In order to study the practical significance of the TCNQ-PdNP-2 modified carbon paste electrode real sample analysis was performed in vitamin C tablets using the standard addition method. The vitamin C tablet was diluted in 0.1 M phosphate buffer solution (pH 7.0). Vitamin C tablet samples were added with 10, 20, and 50 μM ascorbic acid in 0.1 M phosphate buffer solution using an amperometric technique at a fixed potential of 0.22 V vs. Ag/AgCl. The recovery result ranges from 93.60 % to 98.32 % as shown in (Table 3.4). A recovery range within 90 % to 110 % is acceptable in analytical chemistry for complex matrices, meaning that the method provides reliable results in real-time analysis. This recovery range of 93.60 % to 98.32 % signifies that the electrochemical method used for vitamin C tablet analysis is accurate, reliable, and applicable for real sample analysis in pharmaceutical formulations. The method demonstrates minimal matrix effects, high precision, and compliance with regulatory standards, making it suitable for routine quality control and validation purposes in the analysis of vitamin C in commercial tablets.

Table 3.4 Real sample analysis of ascorbic acid in ascorbic acid tablet sample.

Sample No.	Amount used (μM)	*Amount found (μM)	Recovery (%)
1	10	9.36 ± 0.32	93.60
2	20	18.84 ± 0.53	94.20
3	50	49.16 ± 0.16	98.32

*Repeated three times (n =3)

3.4 Conclusions

The current research was undertaken to fasten the dynamic electrochemistry of TCNQ in electrochemical sensing in the presence of palladium in two different nanogeometry. The three different systems, namely CPE/TCNQ, CPE/TCNQ-PdNP-1, and CPE/TCNQ-PdNP-2 electrodes, clearly predict the gradual decrease in charge transfer resistance as a function of palladium nanogeometry. The sluggish electrochemistry of TCNQ-modified electrodes tends to be faster in the presence of palladium, with a gradual increase in terms of peak current as a function of palladium nanogeometry. The TCNQ-modified electrode function was observed to be dependent on palladium nanogeometry even at a faster scan rate. The CPE/TCNQ-PdNP-2 modified electrode showed high sensitivity (14.8 µA/mM), a wide linear range (50-625 µM), and a low detection limit (30.35 µM). Additionally, it shows outstanding reproducibility, storage stability, repeatability, and accuracy in real sample detection. The as-synthesized palladium nanoparticle is cost-effective and widely accessible, making it a viable alternative for low-cost portable sensor manufacturing. This can improve the market competitiveness of commercially available enzyme-free sensors, which currently rely mainly on precious metals for electrode materials.

3.5 References

[1] M. Moretti, D.B. Fraga, A.L.S. Rodrigues, Preventive and therapeutic potential of ascorbic acid in neurodegenerative diseases, CNS Neurosci Ther 23 (2017) 921–929. https://doi.org/10.1111/cns.12767.

[2] M. Berretta, V. Quagliariello, N. Maurea, R. Di Francia, S. Sharifi, G. Facchini, L. Rinaldi, M. Piezzo, M. Ceccarelli, G. Nunnari, M. Montopoli, Multiple effects of ascorbic acid against chronic diseases: Updated evidence from preclinical and clinical studies, Antioxidants 9 (2020) 1–27. https://doi.org/10.3390/antiox9121182.

[3] H. Li, Y. Zhou, J. Du, Ascorbic acid as an alternative coreactant for luminol reaction and sensitive chemiluminescence determination of ascorbic acid in soft drinks, J Photochem Photobiol A Chem 429 (2022) 113945. https://doi.org/10.1016/j.jphotochem.2022.

[4] Y.P. Dong, T.T. Gao, X.F. Chu, J. Chen, C.M. Wang, Flow injection-chemiluminescence determination of ascorbic acid based on luminol-ferricyanide-gold nanoparticles system, J Lumin 154 (2014) 350–355. https://doi.org/10.1016/j.jlumin.2014.05.011.

[5] B. Gómez Ruiz, S. Roux, F. Courtois, C. Bonazzi, Spectrophotometric method for fast quantification of ascorbic acid and dehydroascorbic acid in simple matrix for kinetics measurements, Food Chem 211 (2016) 583–589. https://doi.org/10.1016/j.foodchem.2016.05.107.

[6] K. Shrivas, K. Agrawal, D.K. Patel, A spectrophotometric determination of ascor bic acid, Journal of the Chinese Chemical Society 52 (2005) 503–506. https://doi.org/10.1002/jccs.200500072.

[7] A.I.R.N.A. Barros, A.P. Silva, B. Gonçalves, F.M. Nunes, A fast, simple, and reliable hydrophilic interaction liquid chromatography method for the determination of ascorbic and isoascorbic acids, Anal Bioanal Chem 396 (2010) 1863–1875. https://doi.org/10.1007/s00216-009-3414-4.

[8] V. Gokmen, N. Kahraman, N. Demir, J. Acar, Enzymatically validated liquid chromatographic method for the determination of ascorbic and dehydroascorbic acids in fruit and vegetables Journal of Chromatography A 881 (2000) 309-316. https://doi.org/10.1016/S0021-9673(00)00080-7.

[9] H. Beitollahi, Z. Dourandish, S. Tajik, F. Sharifi, P.M. Jahani, Electrochemical Sensor Based on Ni-Co Layered Double Hydroxide Hollow Nanostructures for Ultrasensitive Detection of Sumatriptan and Naproxen, Biosensors (Basel) 12 (2022) 872. https://doi.org/10.3390/bios12100872.

[10] B. Wu, Y. Kuang, X. Zhang, J. Chen, Noble metal nanoparticles/carbon nanotubes nanohybrids: Synthesis and applications, Nano Today 6 (2011) 75–90. https://doi.org/10.1016/j.nantod.2010.12.008.

[11] A. Esfandiar, S. Ghasemi, A. Irajizad, O. Akhavan, M.R. Gholami, The decoration of TiO2/reduced graphene oxide by Pd and Pt nanoparticles for hydrogen gas sensing, Int J Hydrogen Energy 37 (2012) 15423–15432. https://doi.org/10.1016/j.ijhydene.2012.08.011.

[12] G. huang Wu, Y. fang Wu, X. wei Liu, M. cong Rong, X. mei Chen, X. Chen, An electrochemical ascorbic acid sensor based on palladium nanoparticles supported on graphene oxide, Anal Chim Acta 745 (2012) 33–37. https://doi.org/10.1016/j.aca.2012.07.034.

[13] J. Huang, Y. Liu, H. Hou, T. You, Simultaneous electrochemical determination of dopamine, uric acid and ascorbic acid using palladium nanoparticle-loaded carbon nanofibers modified electrode, Biosens Bioelectron 24 (2008) 632–637. https://doi.org/10.1016/j.bios.2008.06.011.

[14] D. Wen, S. Guo, S. Dong, E. Wang, Ultrathin Pd nanowire as a highly active electrode material for sensitive and selective detection of ascorbic acid, Biosens Bioelectron 26 (2010) 1056–1061. https://doi.org/10.1016/j.bios.2010.08.054.

[15] S. Harish, J. Mathiyarasu, K.L.N. Phani, V. Yegnaraman, PEDOT/Palladium composite material: Synthesis, characterization and application to simultaneous determination of dopamine and uric acid, J Appl Electrochem 38 (2008) 1583–1588. https://doi.org/10.1007/s10800-008-9609-0.

[16] A. Lebon, A. García-Fuente, A. Vega, F. Aguilera-Granja, Hydrogen interaction in Pd-Pt alloy nanoparticles, Journal of Physical Chemistry C 116 (2012) 126–133. https://doi.org/10.1021/jp207329q.

[17] G. Cui, S. Song, P.K. Shen, A. Kowal, C. Bianchini, First-principles considerations on catalytic activity of Pd toward ethanol oxidation, Journal of Physical Chemistry C 113 (2009) 15639–15642. https://doi.org/10.1021/jp900924s.

[18] T. Wang, A. Chutia, D.J.L. Brett, P.R. Shearing, G. He, G. Chai, I.P. Parkin, Palladium alloys used as electrocatalysts for the oxygen reduction reaction, Energy Environ Sci 14 (2021) 2639–2669. https://doi.org/10.1039/d0ee03915b.

[19] E.A. Crespo, M. Ruda, S. Ramos De Debiaggi, E.M. Bringa, F.U. Braschi, G. Bertolino, Hydrogen absorption in Pd nanoparticles of different shapes, in: Int J Hydrogen Energy, 37 (2012) 14831–14837. https://doi.org/10.1016/j.ijhydene.2011.12.075.

[20] M. Alaqarbeh, S.F. Adil, T. Ghrear, M. Khan, M. Bouachrine, A. Al-Warthan, Recent Progress in the Application of Palladium Nanoparticles: A Review, Catalysts 13 (2023) 1343. https://doi.org/10.3390/catal13101343.

[21] W. Li, X. shan Chu, F. Wang, Y. yan Dang, X. yun Liu, X. chuan Wang, C. yi Wang, Enhanced cocatalyst-support interaction and promoted electron transfer of 3D porous g-C3N4/GO-M (Au, Pd, Pt) composite catalysts for hydrogen evolution, Appl Catal B 288 (2021) 120034. https://doi.org/10.1016/j.apcatb.2021.

[22] S. Sarkar, S.C. Peter, An overview on Pd-based electrocatalysts for the hydrogen evolution reaction, Inorg Chem Front 5 (2018) 2060–2080. https://doi.org/10.1039/c8qi00042e.

[23] L. Bruno, M. Scuderi, F. Priolo, L. Falciola, S. Mirabella, Enlightening the bimetallic effect of Au@Pd nanoparticles on Ni oxide nanostructures with enhanced catalytic activity, Sci Rep 13 (2023) 3203. https://doi.org/10.1038/s41598-023-29679-6.

[24] G. huang Wu, Y. fang Wu, X. wei Liu, M. cong Rong, X. mei Chen, X. Chen, An electrochemical ascorbic acid sensor based on palladium nanoparticles supported on graphene oxide, Anal Chim Acta 745 (2012) 33–37. https://doi.org/10.1016/j.aca.2012.07.034.

[25] A.S. N Murthy, Electrochemical oxidation of L-ascorbic acid on 7,7,8,8-tetracyanoquinodimethane (TCNQ) modified electrode Biosensors and Bioelectronics 9 (1994) 439-444. https://doi.org/10.1016/0956-5663(94)90032-9.

[26] Z. Hussain, W. Zou, B.J. Murdoch, A. Nafady, M.R. Field, R. Ramanathan, V. Bansal, Metal–Organic Charge Transfer Complexes of Pb(TCNQ)2 and Pb(TCNQF4)2 as New Catalysts for Electron Transfer Reactions, Adv Mater Interfaces 7 (2020) 2001111. https://doi.org/10.1002/admi.

[27] H. Wang, Q. Wu, Y. Wang, X. Lv, H. guo Wang, A redox-active metal–organic compound for lithium/sodium-based dual-ion batteries, J Colloid Interface Sci 606 (2022) 1024–1030. https://doi.org/10.1016/j.jcis.2021.08.113.

[28] R. Murase, T.A. Hudson, T.S. Aldershof, K. V. Nguyen, J.G. Gluschke, E.P. Kenny, X. Zhou, T. Wang, M.P. Van Koeverden, B.J. Powell, A.P. Micolich, B.F. Abrahams, D.M. D'Alessandro, Multi-Redox Responsive Behavior in a Mixed-Valence Semiconducting Framework Based on Bis-[1,2,5]-thiadiazolo-tetracyanoquinodimethane, J Am Chem Soc 144 (2022) 13242–13253. https://doi.org/10.1021/jacs.2c03794.

[29] G.A. Leith, A.M. Rice, B.J. Yarbrough, A.A. Berseneva, R.T. Ly, C.N. Buck, D. Chusov, A.J. Brandt, D.A. Chen, B.W. Lamm, M. Stefik, K.S. Stephenson, M.D. Smith, A.K. Vannucci, P.J. Pellechia, S. Garashchuk, N.B. Shustova, A Dual Threat: Redox-Activity and Electronic Structures of Well-Defined Donor–Acceptor Fulleretic Covalent-Organic Materials, Angewandte Chemie - International Edition 59 (2020) 6000–6006. https://doi.org/10.1002/anie.201914233.

[30] Y. Fujihara, Y. Fujihara, H. Kobayashi, S. Takaishi, T. Tomai, M. Yamashita, I. Honma, Electrical Conductivity-Relay between Organic Charge-Transfer and Radical Salts toward Conductive Additive-Free Rechargeable Battery, ACS Appl Mater Interfaces 12 (2020) 25748–25755. https://doi.org/10.1021/acsami.0c03642.

[31] H. Peng, S. Huang, D. Tranca, F. Richard, W. Baaziz, X. Zhuang, P. Samorì, A. Ciesielski, Quantum Capacitance through Molecular Infiltration of 7,7,8,8-Tetracyanoquinodimethane in Metal-Organic Framework/Covalent Organic Framework Hybrids, ACS Nano 15 (2021) 18580–18589. https://doi.org/10.1021/acsnano.1c09146.

[32] P.C. Pandey, V. Pandey, S. Mehta, An for amperometric enzyme electrode lactate based on graphite paste modified with tetracyanoquinodimethane Biosensors and Bioelectronics 9 (1994) 365-372. https://doi.org/10.1016/0956-5663(94)80037-5.

[33] I. Ivanov, T. Vidaković-Koch, K. Sundmacher, Alternating electron transfer mechanism in the case of high-performance tetrathiafulvalene-tetracyanoquinodimethane enzymatic electrodes, Journal of Electroanalytical Chemistry 690 (2013) 68–73. https://doi.org/10.1016/j.jelechem.2012.11.009.

[34] H. Wu, C. Tian, X. Song, C. Liu, D. Yang, Z. Jiang, Methods for the regeneration of nicotinamide coenzymes, Green Chemistry 15 (2013) 1773–1789. https://doi.org/10.1039/c3gc37129h.

[35] R. Sato, T. Kawamoto, T. Mori, Asymmetrical hole/electron transport in donor-acceptor mixed-stack cocrystals, J Mater Chem C Mater 7 (2019) 567–577. https://doi.org/10.1039/c8tc05190a.

[36] P.C. Pandey, S. Upadhyay, B.C. Upadhyay, H.C. Pathak, Ethanol Biosensors and Electrochemical Oxidation of NADH Analytical Biochemistry 260 (1998) 195-203. https://doi.org/10.1006/abio.1998.2679.

[37] P.C. Pandey, R. Singh, A.K. Pandey, Tetrahydrofuran hydroperoxide and 3-aminopropyltrimethoxysilane mediated controlled synthesis of Pd, Pd-Au, Au-Pd nanoparticles: Role of Palladium nanoparticles on the redox electrochemistry of ferrocene monocarboxylic acid, Electrochim Acta 138 (2014) 163–173. https://doi.org/10.1016/j.electacta.2014.06.101.

[38] P.C. Pandey, S. Upadhyay, I. Tiwari, S. Sharma, A novel ferrocene-encapsulated palladium-linked ormosil-based electrocatalytic biosensor. The role of the reactive functional group, Electroanalysis 13 (2001) 1519–1527. https://doi.org/10.1002/1521-4109(200112)13:18

[39] P.C. Pandey, S. Upadhyay, N.K. Shukla, S. Sharma, Studies on the electrochemical performance of glucose biosensor based on ferrocene encapsulated ORMOSIL and glucose oxidase modified graphite paste electrode, Biosens Bioelectron 18 (2003) 1257–1268. https://doi.org/10.1016/S0956-5663(03)00075-7.

[40] P.C. Pandey, R. Singh, Controlled synthesis of Pd and Pd-Au nanoparticles: Effect of organic amine and silanol groups on morphology and polycrystallinity of nanomaterials, RSC Adv 5 (2015) 10964–10973. https://doi.org/10.1039/c4ra16201c.

[41] P.C. Pandey, G. Pandey, J. Haider, G. Pandey, Role of organic carbonyl moiety and 3-aminopropyltrimethoxysilane on the synthesis of gold nanoparticles specific to pH- and salt-tolerance, J Nanosci Nanotechnol 16 (2016) 6155–6163. https://doi.org/10.1166/jnn.2016.11104.

[42] C.M. Kuskur, B.E. Kumara Swamy, H. Jayadevappa, P.S. Ganesh, Poly (rhodamine B) sensor for norepinephrine and paracetamol: a voltammetric study, Ionics (Kiel) 24 (2018) 3631–3640. https://doi.org/10.1007/s11581-018-2483-9.

[43] N. Kumar, Rosy, R.N. Goyal, Palladium nano particles decorated multi-walled carbon nanotubes modified sensor for the determination of 5-hydroxytryptophan in biological fluids, Sens Actuators B Chem 239 (2017) 1060–1068. https://doi.org/10.1016/j.snb.2016.08.122.

[44] P. Wu, Y. Huang, X. Zhao, D. Lin, L. Xie, Z. Li, Z. Zhu, H. Zhao, M. Lan, MnFe2O4/MoS2 nanocomposite as Oxidase-like for electrochemical simultaneous detection of ascorbic acid, dopamine and uric acid, Microchemical Journal 181 (2022) 107780. https://doi.org/10.1016/j.microc.2022.

[45] L. Yang, D. Liu, J. Huang, T. You, Simultaneous determination of dopamine, ascorbic acid and uric acid at electrochemically reduced graphene oxide modified electrode, Sens Actuators B Chem 193 (2014) 166–172. https://doi.org/10.1016/j.snb.2013.11.104.

[46] H. Huang, Y. Yue, Z. Chen, Y. Chen, S. Wu, J. Liao, S. Liu, H. rui Wen, Electrochemical sensor based on a nanocomposite prepared from TmPO 4 and graphene oxide for simultaneous voltammetric detection of ascorbic acid, dopamine and uric acid, Microchimica Acta 186 (2019) 1-9. https://doi.org/10.1007/s00604-019-3299-7.

[47] W. Kit-Anan, A. Olarnwanich, C. Sriprachuabwong, C. Karuwan, A. Tuantranont, A. Wisitsoraat, W. Srituravanich, A. Pimpin, Disposable paper-based electrochemical sensor utilizing inkjet-printed Polyaniline modified screen-printed carbon electrode for Ascorbic acid detection, Journal of Electroanalytical Chemistry 685 (2012) 72–78. https://doi.org/10.1016/j.jelechem.2012.08.039.

[48] W. Chen, J. Tang, H.J. Cheng, X.H. Xia, A simple method for fabrication of sole composition nickel hexacyanoferrate modified electrode and its application, Talanta 80 (2009) 539–543. https://doi.org/10.1016/j.talanta.2009.07.022.

[49] P.L. dos Santos, V. Katic, K.C.F. Toledo, J.A. Bonacin, Photochemical one-pot synthesis of reduced graphene oxide/Prussian blue nanocomposite for simultaneous electrochemical detection of ascorbic acid, dopamine, and uric acid, Sens Actuators B Chem 255 (2018) 2437–2447. https://doi.org/10.1016/j.snb.2017.09.036.

[50] K. Ghanbari, N. Hajheidari, ZnO-CuxO/polypyrrole nanocomposite modified electrode for simultaneous determination of ascorbic acid, dopamine, and uric acid, Anal Biochem 473 (2015) 53–62. https://doi.org/10.1016/j.ab.2014.12.013.

[51] U. Rajaji, P.S. Ganesh, S.M. Chen, M. Govindasamy, S.Y. Kim, R. A. Alshgari, G. Shimoga, Deep eutectic solvents synthesis of perovskite type cerium aluminate embedded carbon nitride catalyst: High-sensitive amperometric platform for sensing of glucose in biological fluids, Journal of Industrial and Engineering Chemistry 102 (2021) 312–320. https://doi.org/10.1016/j.jiec.2021.07.015.